Geophysical Research Letters

RESEARCH LETTER
10.1029/2022GL101633

Gigantic Vortices From Barotropic Instability Observed in the Atmosphere of Venus

Takeshi Horinouchi[1], **Takehiko Satoh**[2], **and Javier Peralta**[3]

[1]Faculty of Environmental Earth Science, Hokkaido University, Sapporo, Japan, [2]Institute of Space and Astronautical Science, JAXA, Sagamihara, Japan, [3]Facultad de Física, Universidad de Sevilla, Sevilla, Spain

Key Points:

- An event of barotropic instability, whose scale is greater than 1,000 km, was found by the Akatsuki Venus orbiter
- The discovery reinforces the recent view that the lower to middle cloud regions are dynamically active, promoting further studies

Correspondence to:

T. Horinouchi,
horinout@ees.hokudai.ac.jp

Citation:

Horinouchi, T., Satoh, T., & Peralta, J. (2023). Gigantic vortices from barotropic instability observed in the atmosphere of Venus. *Geophysical Research Letters*, *50*, e2022GL101633. https://doi.org/10.1029/2022GL101633

Received 13 OCT 2022
Accepted 27 DEC 2022

Author Contributions:

Conceptualization: Takeshi Horinouchi
Data curation: Takehiko Satoh
Formal analysis: Takeshi Horinouchi
Investigation: Takeshi Horinouchi, Javier Peralta
Methodology: Takeshi Horinouchi
Project Administration: Takehiko Satoh
Resources: Takehiko Satoh
Software: Takeshi Horinouchi
Validation: Takeshi Horinouchi, Takehiko Satoh
Visualization: Takeshi Horinouchi
Writing – original draft: Takeshi Horinouchi
Writing – review & editing: Takehiko Satoh, Javier Peralta

Abstract Until recently, the lower to middle cloud region of Venus had been supposed to be dynamically quiet, accommodating nearly steady superrotating westward flow. However, observations of the regions by Akatsuki, the latest Venus orbiter operating since 2015, have revealed a variety of cloud features indicative of vortices and waves. Here we report another, and arguably the most conspicuous, example. Akatsuki's near-infrared imager IR2 captured gigantic vortices rotating cyclonically on 25 August 2016. By using winds estimated by cloud tracking, the feature is shown to be quantitatively consistent with barotropic instability. The size of the vortices (~1,000 km) and their spacing (~2,500 km) are more than several times greater than the vortex-like features reported previously from the observations of Venus, and they are also greater than the largest barotropic instability observed in the Earth's troposphere.

Plain Language Summary Hydrodynamical instabilities play important roles in the general circulation of the Earth and planetary atmospheres. Barotropic instability is a kind of instability that arises from horizontal differences in predominantly parallel horizontal flows. We report herewith the first concrete evidence of its occurrence in the atmosphere of Venus. Before this study, reports are limited to vortex-like cloud features whose appearance is consistent with this instability, but no analyses of flows have been conducted before. The cloud feature like a vortex street reported in this study has a spatial scale far greater than any of previously reported ones, and our study shows that it is dynamically consistent with barotropic instability.

1. Introduction

Venus is covered with thick clouds extending typically from about 48 to 70 km altitude. The cloud layer can be divided to two regimes: one from the bottom to ~57 km is strongly affected by heating due to the thermal radiation from the hot ground/atmosphere (the lower to middle cloud region), and another from ~57 km to the top (the upper cloud region) is primarily controlled by the solar insolation. Until recently, the lower to middle cloud region had been supposed to be dynamically quiet, accommodating nearly steady westward superrotating flows with little variability (Hueso et al., 2012; Peralta et al., 2018; Sánchez-Lavega et al., 2008). Akatsuki, the latest Venus orbiting satellite operating since December 2015 (Nakamura et al., 2016), changed this view. From its night-side imaging observations at near-infrared wavelengths around 2 μm, which visualizes lower-to-middle clouds illuminated by deep thermal radiation (see the first paragraph of Section 2 for further information), it was found that the westward wind near the equator was sped up by ~20 m/s over a monthly time scale to form a feature named the equatorial jet (Horinouchi, Murakami, Satoh, et al., 2017: H17, hereinafter). The Akatsuki images revealed a wide variety of cloud features consistent with vortices and waves at scales ranging from 100 to 1,000 km (Limaye et al., 2018; Peralta et al., 2019). Peralta et al. (2020) reported a discontinuous feature in the lower to middle cloud region that circulates at a period around 4.9 terrestrial days, which is likely a part of a planetary-scale wave. Among these cloud features, particularly related to this study is the one resembling a vortex street created by barotropic instability (Peralta et al., 2019); the images taken on 13 August 2016 by the IR2 instrument onboard Akatsuki (Satoh et al., 2017) captured five vortex-like features aligned at intervals around 800 km (their Figure 1e). Peralta et al. (2019) also found similar examples with smaller scales (their Figure 1dg). Earlier studies examined zonal flows obtained from cloud-top images (Travis, 1978) and from radio occultation (Michelangeli et al., 1987) and suggested possible occurrence of barotropic instability.

Barotropic instability is associated with horizontal shear and is a kind of the inflection-point instability extended to include the beta effect (H. L. Kuo, 1949; Rayleigh, 1880). This instability breaks up a shear of a parallel flow into vortices (also called as billows). In the Earth's atmosphere, unstable billows are frequently observed from

the Kelvin-Helmholtz (KH) instability, which occurs at the boundary of two vertically adjacent fluid layers with different velocities and densities. Generally, the horizontal scales of atmospheric motions tend to be much greater than the vertical scales, so cloud visualization of barotropic instability is available only for satellites, and such reports are limited (H.-C. Kuo & Horng, 1994; Maejima et al., 2006). To the authors' knowledge, the largest vortex street that has been identified in the Earth's troposphere and attributed to be arising from barotropic instability is the inter-tropical-convergence-zone (ITCZ) breakdown observed in 1988 (Ferreira & Schubert, 1997; Hack et al., 1989). In this spectacular event, the horizontal shear was built up by low-level convergence and updraft in the ITCZ. The flow then became barotropically unstable, and the sheared region, having strong cyclonic vorticity, was torn apart to turn into several vortices at intervals around 1,300 km. The vortices further developed into intense tropical cyclones. Actually, smaller-scaled (and less spectacular) barotropic instability to create tropical cyclones occurs frequently at ITCZ (e.g., Fudeyasu et al., 2022; Ritchie & Holland, 1999). Barotropic instability has been suggested to occur in the Earth's middle atmosphere as well, possibly with spatial scales greater than those in the troposphere (e.g., Hartmann, 1983). See Read et al. (2020) for possible barotropic instabilities in the atmosphere of other planets.

In this paper, we report the largest vortex street observed in the atmosphere of Venus on 25 August 2016. Its size is greater than the giant ITCZ breakdown reported for the Earth. We attribute the vortices as arising from barotropic instability. This discovery further cast questions for future studies, as it is unclear how the instability can be created.

2. Data and Methods

As in the earlier studies introduced above (H17; Limaye et al., 2018; Peralta et al., 2018, 2019; 2020), we used the nightside images obtained by IR2 at the wavelength of 2.26 μm. This wavelength is in the so-called near-infrared window at which thermal infrared from the lower part of the atmosphere partly escapes to space (Allen & Crawford, 1984), and the images capture silhouettes of clouds. These silhouettes are supposed to represent morphology of clouds in the lower to middle cloud region, because they are optically thicker than upper clouds, and because the upper clouds are likely more horizontally uniform because of the higher static stability; comparison of velocities obtained by tracking the near-infrared features and the velocities obtained from entry probes and radio-occultation observations supports it (e.g., Allen & Crawford, 1984; Hueso et al., 2012).

Observations of Venus' night-side by IR2 began in March 2016 and continued until November 2016, the time when malfunctioning of the control electronics happened (early December 2016). The acquisition of images was normally conducted every 2 hr, but imaging on 25 August 2016, was conducted exceptionally at a 1-hr interval. Nightside images obtained from 04 to 22 UTC, 25 August 2016, were processed to reduce contamination of the reflected solar radiation from the dayside (Satoh et al., 2021). Akatsuki was moving away from Venus on the day; the sub-spacecraft-point image resolution was 19 km at 04 UTC, and it was 39 km at 22 UTC. We also used data on other days for visual inspection and cloud tracking; these data were used without the optical correction. Note that in our study, inaccuracy in photometry does not affect results, since we rely on relative contrasts. The optical correction for the 25 August data was done to improve image quality near the day-night boundary.

We derived winds by tracking cloud features on 20 and 25 August 2016 by using the method described in Ikegawa and Horinouchi (2016) and Horinouchi, Murakami, Kouyama, et al. (2017). The sub-spacecraft-point image resolutions on 20 August were 68–73 km. The wind data for 20 August were derived from the images mapped geographically by using the planetary limb fitting described in H17. Cloud tracking was conducted by using four consecutive images obtained over 6 hr at the interval of 2 hr. Each of the wind estimation (vector) represents motion of small-scale cloud features over a $\sim 10^\circ \times 10^\circ$ region. As in H17, wind estimations were derived on a 3° grid both in longitude and latitude, so it is over-sampling. The threshold value of the screening parameter of the deformation consistency α in Horinouchi, Murakami, Kouyama, et al. (2017) is set to 1.

The images obtained on 25 August were mapped slightly differently. The navigation information for each image was first corrected using the method by H17. However, the planetary limb on this day was exceptionally obscure, so the quality of the navigation correction was relatively low, and the resultant geographically mapped images exhibited some fluctuation over time. We therefore applied the cloud tracking for each of the adjacent one-hourly image pairs, and the results were used to compensate the fluctuation appearing in the mean motion. We then re-mapped the images from 5 to 21 UTC, unchanging the mapping of the first (4 UTC) and the last (22 UTC)

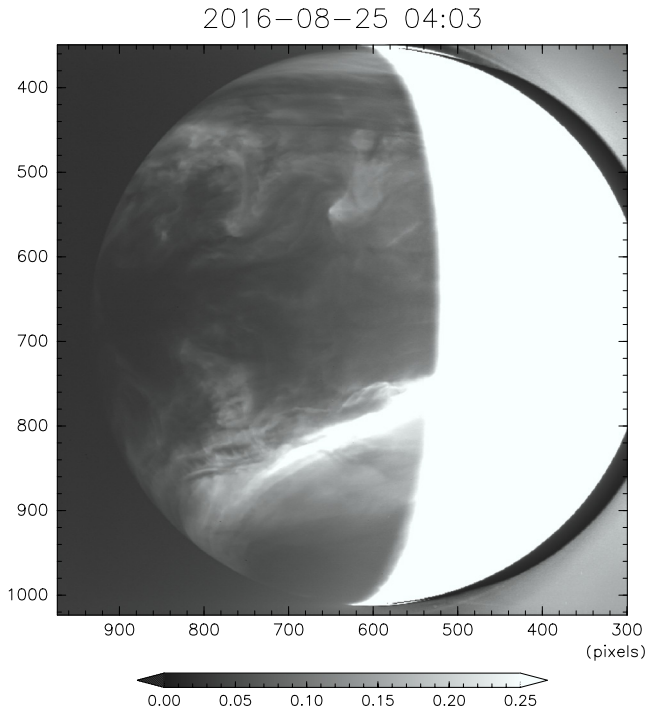

Figure 1. The contamination-reduced 2.26-μm radiance (W m^{-2} sr^{-1} m^{-1}) at 4 UTC, 25 August 2016.

images. This correction does not change mean winds over the day, and it improves consistency among mappings. The corrected images were used for cloud tracking. As in H17, the images obtained over 6 hr were used, but for this day, seven images were used because the imaging was conducted one-hourly. The deformation consistency threshold is tightened to 0.5 to reduce the artifacts of linear-shaped features (see Section 3) prevalent in the images of the day, although some artifacts remained as described Section 3.

The precision of wind estimation is evaluated by the parameter named ε in Ikegawa and Horinouchi (2016) for each grid point. It does not ensure accuracy, but overall, it empirically corresponds roughly to the one-to-two times the errors estimated directly from the consistency among wind estimations (Horinouchi et al., 2020). The ε values obtained in the present study are described in what follows.

3. Results

Figure 1 shows an example of the IR2 2.26-μm images on 25 August 2016, and Figure 2 shows an hourly geographically-mapped time sequence, where color shading is reverted. At 04 UTC (upper-left), two relatively dark (less opaque) features that look like vortices arising from barotropic instability exist at around 100°E and 125°E; the scale of the vortex-like features is around 1,000 km. Note that the gray-scale shading is made brighter for lower radiance, which indicates lower opacity and hence optically thicker clouds. The vortex-like features, which are relatively dark in the figure, are thus relatively less clouded. Another seemingly similar dark region is found at around 80°E, 10°N, but it is very faint, so we will not treat it in what follows.

The subsequent panels in Figure 2 were created by shifting longitude westward at the angular speed corresponding to 75 m s^{-1} at the equator. The features move little in the figure, so they actually move westward at around 60° per day. The overall westward speed is consistent with the earlier observations of the superrotation in the lower to middle cloud region (Sánchez-Lavega et al., 2008; Hueso et al., 2012; H17; Peralta et al., 2018). Barotropic instability consists of horizontal motion, and there is no necessity for its resultant vortices to have lower or higher cloud opacity. It appears that the low opacity in the vortex-like feature is due to advection from the belt of low opacity between 20° and 30°N. The two vortex-like features appear somewhat vague in later images of the time series. This change may have been caused by thickening of the clouds. However, it should be noted that the IR2 night-side data are affected by the contamination from the day crescent due to the instrumental point-spread function (Satoh et al., 2017). Distinguishing intrinsic changes of clouds and the instrumental effects require cleaning of the data and detailed radiative transfer analysis which are out of scope of this work.

Among the two vortex-like features in Figure 2, the one on the right, which was at around 125°E at 04 UTC, was deformed with time. The hook-like feature whose tip was at ∼108°E, 10°N at 04 UTC, was gradually expanded westward. The overall change of its shape suggests clockwise rotation, which is cyclonic in the case of the northern hemisphere under the retrograde rotation. On the other hand, the vortex-like feature on the left, located at ∼100°E at 04 UTC, is more obscure from the initial time, and its morphological change is unclear.

Horizontal winds obtained by using the seven images since 8 UTC are shown in Figure 3 as the deviation from a solid-body rotation. The winds obtained by using images starting at different times were similar, so the description in what follows is robust. The estimated winds do exhibit clockwise (cyclonic) rotation on the vortex-like feature on the right. The values of the precision measure ε are 2–4 m s^{-1} on this feature, which is below the velocity contrast therein. The Okubo-Weiss parameter (Okubo, 1970) computed around the feature exhibited negative values (not shown), indicating consistency with vortical motion. On the other hand, the estimated winds over the vortex-like feature on the left are not very consistent with vortical motion. This may be because the feature is too obscure. The northward flow at around 90°E, 25°N is likely an artifact arising from the northward migration of a linear-shaped whiter feature extending southwest to northeast. This kind of feature is named as "dark streaks" by Peralta et al. (2019) from their relatively fewer radiance; their simple linear shape indicates that it might be associated with the propagation of a wave rather than the advection of clouds.

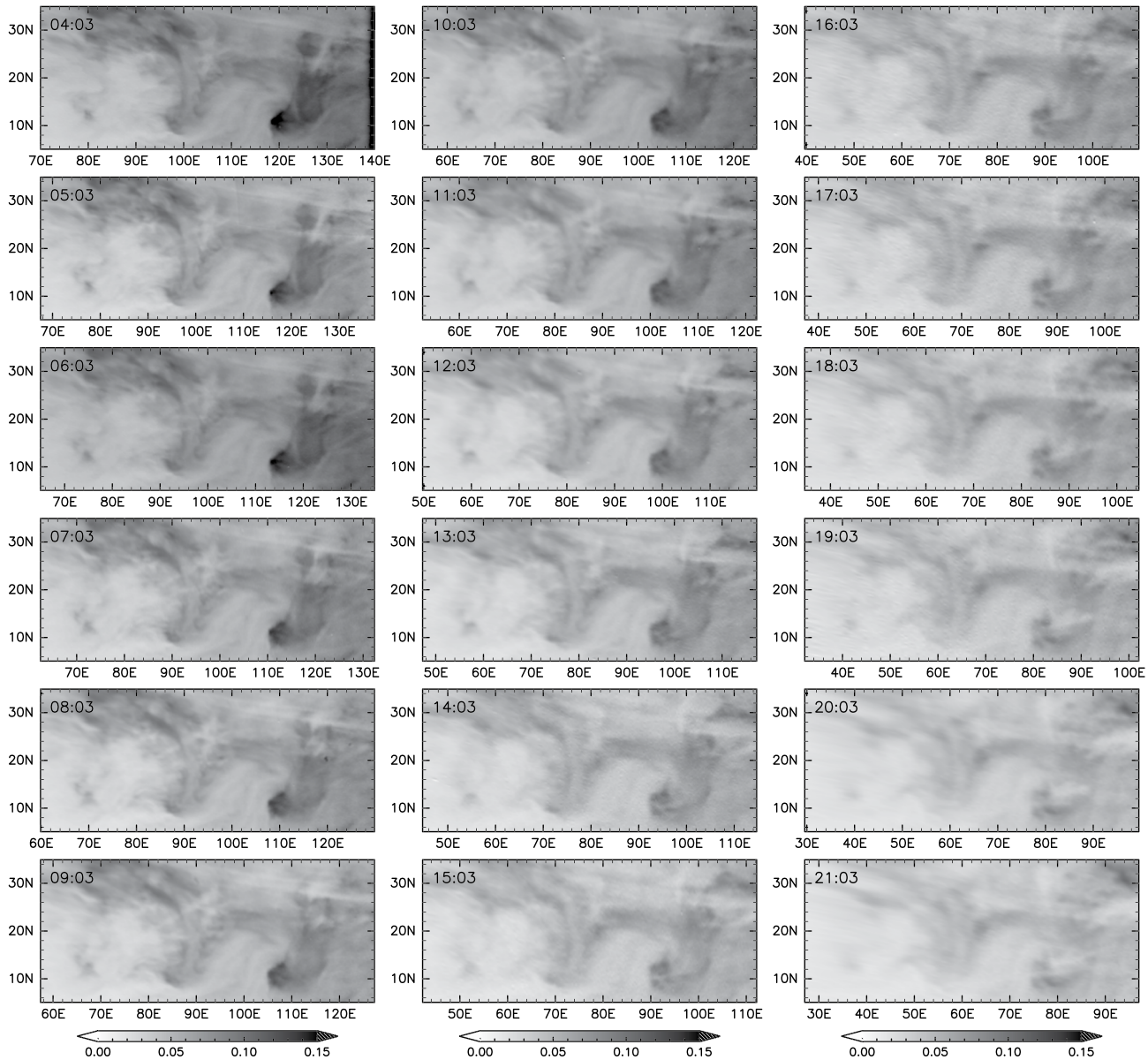

Figure 2. Hourly sequence of the 2.26-μm radiance ($W\,m^{-2}\,sr^{-1}\,m^{-1}$; color shading is the whiter for the darker) obtained on 25 August 2016. Imaging time (UTC) is

We now examine the background mean flow. Figure 4b shows zonally-averaged profiles of the zonal component (negative if westward) of the winds exhibited in Figure 3. The mean zonal flow displays a nearly linear shear between the equator and 35°N. In contrast, the mean zonal flow obtained from the observation on 20 August (Figure 4a) exhibits a strong clockwise shear at around 20°N, forming an inflection point suitable for barotropic instability (here, the mean ε values over 10°–30°N is 8 $m\,s^{-1}$, which is twice as that on 25 August, so the precision of individual cloud-tracking results is relatively low. However, the standard error becomes more than halved because of zonal averaging, and we obtain similar results by using different set of images on the day. Therefore, the existence of the inflection point is robust). The barotropically unstable state on 20 August is also evident in the absolute vorticity (Figure 4a, red curve) whose meridional gradient changes its sign at around the inflection point. The IR2 images on this day were obtained at longitudes roughly 40° to the east compared with those on 25 August. Thus, the region observed on 20 August are around 320° (= 360° − 40°) to the upstream of the region observed on 25 August, indicating that they represent motions of air masses close to each other if advected by 60° per day. The results are qualitatively consistent with the hypothesis that the vortices observed on 25 August

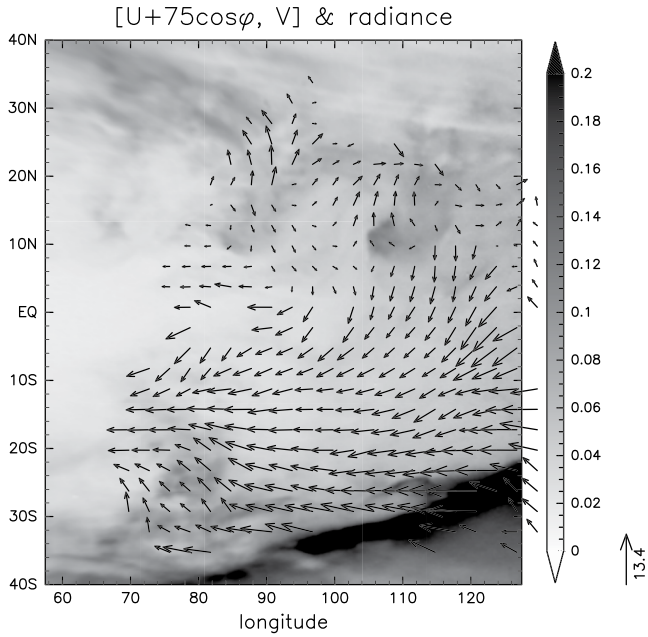

Figure 3. Arrows: horizontal wind deviations from the westward solid body rotation at the speed of 75 $\mathrm{m\,s^{-1}}$ at the equator. The winds are derived from the seven images from 08 to 14 UTC, 25 August 2016; the grid points are defined in terms of the image at 08 UTC. The length scale of the arrows is shown on the lower-right margin in $\mathrm{m\,s^{-1}}$. Gray-scale shading: the 2.26 μm radiance at 08 UTC ($\mathrm{W\,m^{-2}\,sr^{-1}\,m^{-1}}$).

are created by barotropic instability, which was initiated several days before when there was a strong shear. The smoothness of the mean wind on 25 August is explained as the result of stirring by the vortices.

We further examine quantitative consistency. Note that the planetary beta effect is negligible for Venus, since its rotation is very slow with the period of 243 days. A simplest model of barotropically unstable flows is the two-point piecewise-linear flow shown in Figure 5, for which analytic solutions are described in textbooks (e.g., Section 9.2.4 of Vallis, 2017; note that smoothing the sharp bending does not change the solution much). Here we set the width of the sheared region as w and the flow speed difference across the region as $2U_0$. The flow has exponentially growing unstable modes at the wavelengths along the flow greater than $5.0w$. The most unstable mode has the wavelength of $7.9w$, at which the e-folding time is $2.5U_0^{-1}w$. The observed two vortices were separated by around 2,500 km. If we suppose that it corresponds to the most unstable wavelength of $7.9w$, w is found to be 3.2×10^2 km. The width of 320 km is narrower than the sheared region in Figure 4a, but since the resolution of the cloud tracking is around 1,000 km and the profile does not necessarily capture the undisturbed initial condition, it is possible that the sheared region was actually narrower at a certain time. If we further set $U_0 = 10\,\mathrm{m\,s^{-1}}$, the e-folding time is 0.91 day, indicating that the unstable disturbance can grow by 10 times in 2 days. Therefore, it is possible for billows to form and become matured in a few days. These estimates suggest that the vortex-like features can indeed be explained as the vortices arising from barotropic instability.

4. Discussion

The initiation of barotropic instability requires the formation of a narrow sheared region. As for the ITCZ breakdown on the Earth, low-level

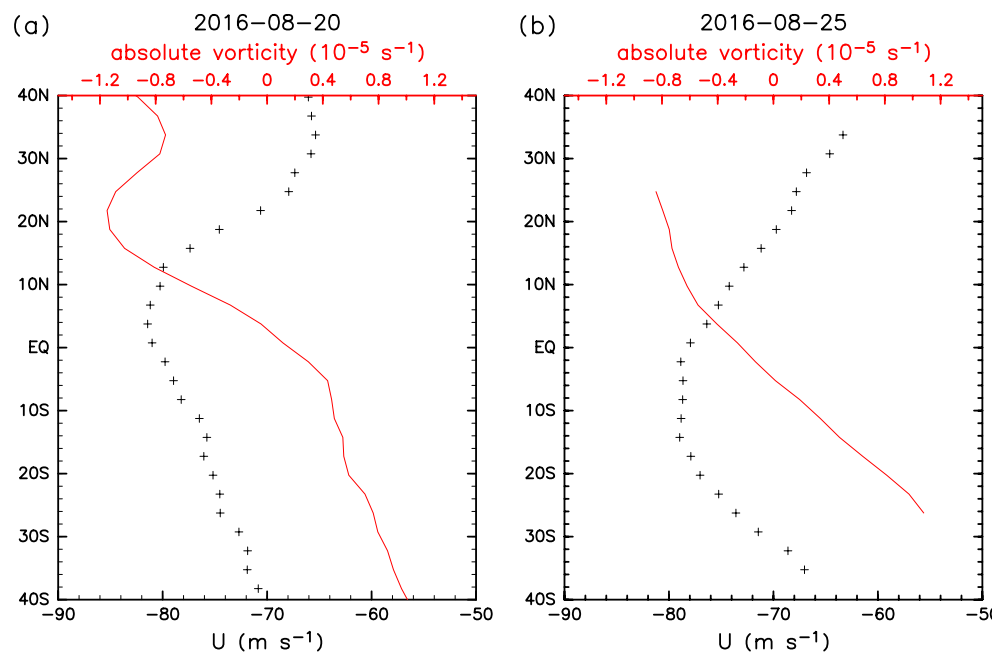

Figure 4. (Black crosses) zonal-mean zonal winds obtained from the 2.26 μm images obtained at (a) 15 to 21 UTC, 20 August 2016, and (b) 08 to 14 UTC, 25 August 2016. (Red curves) absolute vorticity computed from the mean zonal winds by using a central differentiation on the spherical geometry and smoothed by a 5-point running mean (which trims the latitudinal extent of the results).

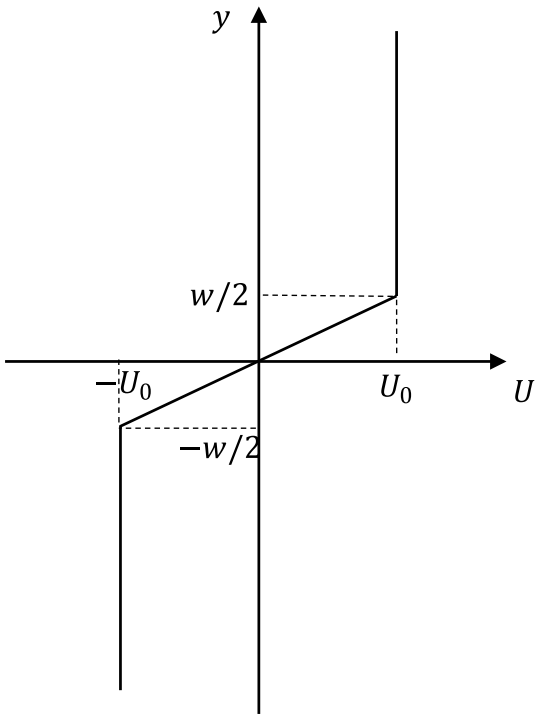

Figure 5. Schematic illustration of a barotropically unstable piecewise linear flow profile.

convergence is driven by intense latent heat release by cumulus convection. On Venus, the main driver of convection is not thought to be the latent heat release but radiation (e.g., Imamura & Hashimoto, 1998). How the large-scale barotropic instability like the present one can be initiated in the cloud region of Venus is left for future studies.

Numerical modeling studies of the Venusian atmosphere also suggest the occurrence of baroclinic instability in the cloud region of Venus at mid to high latitudes (e.g., Sugimoto et al., 2014). Even though we have provided evidence that the vortex street reported in this study is not only qualitatively but also quantitatively consistent with barotropic instability, one could still argue that it may be attributed to baroclinic instability to some extent. Here we discuss this issue. Both instabilities are associated with the meridional gradient of potential vorticity and can create vortices in horizontal motions. The Charney-Stern theorem (Charney & Stern, 1962) unifies the two instabilities, showing that both are associated with a basic state in which the gradient changes its sign somewhere inside the fluid or on its boundary. While barotropic instability is related to the interaction across horizontally adjacent regions with positive and negative gradients, baroclinic instability is related to that across vertically adjacent regions. In the real atmosphere, these two are not mutually exclusive. This is especially the case when a limited region of positive (negative) potential-vorticity gradients is surrounded by environment with negative (positive) gradients. Therefore, distinction can only be made whether the nature of an instability is more consistent with one of the two instability kinds. The case we studied might have baroclinic aspects, but the analysis shown in Section 3 strongly suggests that the primary nature of the vortex formation is barotropic instability.

5. Conclusions

We have shown that the IR2 camera onboard Akatsuki captured gigantic vortex-like features on 25 August 2016. From a comparison of winds on the day and a preceding day, and from a quantitative order estimation, it is shown that they are explained as arising from barotropic instability. Its spatial scale is by far greater than those of previously reported unstable vortex-like features on Venus, and it is greater than that of the largest vortices arising from barotropic instability observed in the Earth's troposphere. The present finding raises a question on how such instability can be initiated in the atmosphere of Venus.

Conflict of Interest

The authors declare no conflicts of interest relevant to this study.

Data Availability Statement

Image data of Akatsuki is publicly available from the AKATSUKI Science Data Archive site https://darts.isas.jaxa.jp/planet/project/akatsuki/ (https://darts.isas.jaxa.jp/doi/vco/vco-00018.html for image data and https://darts.isas.jaxa.jp/doi/vco/vco-00020.html for wind data).

Acknowledgments
The authors thank our numerous colleagues who contributed to create and operate the Akatsuki spacecraft. We also thank the two anonymous reviewers for providing valuable comments. TH thanks the grant in aid JSPS 19H05605. JP thanks funding by the program EMERGIA, Junta de Andalucía (Spain), Grant EMERGIA20_00414.

References

Allen, D. A., & Crawford, J. W. (1984). Cloud structure on the dark side of Venus. *Nature*, *307*(5948), 222–224. https://doi.org/10.1038/307222a0

Charney, J. G., & Stern, M. E. (1962). On the stability of internal baroclinic jets in a rotating atmosphere. *Journal of the Atmospheric Sciences*, *19*(2), 159–172. https://doi.org/10.1175/1520-0469(1962)019<0159:OTSOIB>2.0.CO;2

Ferreira, R. N., & Schubert, W. H. (1997). Barotropic aspects of ITCZ breakdown. *Journal of the Atmospheric Sciences*, *54*(2), 261–285. https://doi.org/10.1175/1520-0469(1997)054<0261:BAOIB>2.0.CO;2

Fudeyasu, H., Shimada, U., Oikawa, Y., Eito, H., Wada, A., Yoshida, R., & Horinouchi, T. (2022). Contributions of the large-scale environment to the typhoon Genesis of Faxai (2019). *Journal of the Meteorological Society of Japan Ser. II*, *100*(4), 617–630. https://doi.org/10.2151/jmsj.2022-031

Hack, J. J., Schubert, W. H., Stevens, D. E., & Kuo, H.-C. (1989). Response of the Hadley circulation to convective forcing in the ITCZ. *Journal of the Atmospheric Sciences*, *46*(19), 2957–2973. https://doi.org/10.1175/1520-0469(1989)046<2957:ROTHCT>2.0.CO;2

Hartmann, D. L. (1983). Barotropic instability of the polar night jet stream. *Journal of the Atmospheric Sciences*, *40*(4), 817–835. https://doi.org/10.1175/1520-0469(1983)040<0817:BIOTPN>2.0.CO;2

Horinouchi, T., Hayashi, Y.-Y., Watanabe, S., Yamada, M., Yamazaki, A., Kouyama, T., et al. (2020). How waves and turbulence maintain the super-rotation of Venus' atmosphere. *Science*, *368*(6489), 405–409. https://doi.org/10.1126/science.aaz4439

Horinouchi, T., Murakami, S., Kouyama, T., Ogohara, K., Yamazaki, A., Yamada, M., & Watanabe, S. (2017). Image velocimetry for clouds with relaxation labeling based on deformation consistency. *Measurement Science and Technology*, *28*(8), 085301. https://doi.org/10.1088/1361-6501/aa695c

Horinouchi, T., Murakami, S., Satoh, T., Peralta, J., Ogohara, K., Kouyama, T., et al. (2017). Equatorial jet in the lower to middle cloud layer of Venus revealed by Akatsuki. *Nature Geoscience*, *10*(9), 646–651. https://doi.org/10.1038/ngeo3016

Hueso, R., Peralta, J., & Sánchez-Lavega, A. (2012). Assessing the long-term variability of Venus winds at cloud level from VIRTIS–Venus Express. *Icarus*, *217*(2), 585–598. https://doi.org/10.1016/j.icarus.2011.04.020

Ikegawa, S., & Horinouchi, T. (2016). Improved automatic estimation of winds at the cloud top of Venus using superposition of cross-correlation surfaces. *Icarus*, *271*, 98–119. https://doi.org/10.1016/j.icarus.2016.01.018

Imamura, T., & Hashimoto, G. L. (1998). Venus cloud formation in the meridional circulation. *Journal of Geophysical Research*, *103*(E13), 31349–31366. https://doi.org/10.1029/1998JE900010

Kuo, H.-C., & Horng, C.-H. (1994). A study of finite amplitude barotropic instability. *Terrestrial, Atmospheric and Oceanic Sciences*, *5*(2), 199–243. https://doi.org/10.3319/tao.1994.5.2.199(tamex)

Kuo, H.-L. (1949). Dynamical instability of two-dimensional nondivergent flow in a barotropic atmosphere. *Journal of Meteorology*, *4*(2), 105–122. https://doi.org/10.1175/1520-0469(1949)006<0105:DIOTDN>2.0.CO;2

Limaye, S., Watanabe, S., Yamazaki, A., Yamada, M., Satoh, T., Sato, T. M., et al. et al. (2018). Venus looks different from day to night across wavelengths: Morphology from Akatsuki multispectral images. *Earth Planets and Space*, *70*(1), 24. https://doi.org/10.1186/s40623-018-0789-5

Maejima, Y., Iga, K., & Niino, H. (2006). Upper-tropospheric vortex street and its formation mechanism. *SOLA*, 2, 80–83. https://doi.org/10.2151/sola.2006-021

Michelangeli, D. V., Zurek, R. W., & Elson, L. S. (1987). Barotropic instability of midlatitude zonal jets on Mars, Earth and Venus. *Journal of the Atmospheric Sciences*, *44*(15), 2031–2041. https://doi.org/10.1175/1520-0469(1987)044<2031:BIOMZJ>2.0.CO;2

Nakamura, M., Imamura, T., Ishii, N., Abe, T., Kawakatsu, Y., Hirose, C., et al. (2016). AKATSUKI returns to Venus. *Earth Planets and Space*, *68*(1), 75. https://doi.org/10.1186/s40623-016-0457-6

Okubo, A. (1970). Horizontal dispersion of floatable particles in the vicinity of velocity singularities such as convergences. *Deep-Sea Research*, *17*(3), 445–454. https://doi.org/10.1016/0011-7471(70)90059-8

Peralta, J., Muto, K., Hueso, R., Horinouchi, T., Sánchez-Lavega, A., Murakami, S. Y., et al. (2018). Nightside winds at the lower clouds of Venus with Akatsuki/IR2: Longitudinal, local time, and decadal variations from comparison with previous measurements. *The Astrophysical Journal - Supplement Series*, *239*(2), 29. https://doi.org/10.3847/1538-4365/aae844

Peralta, J., Navarro, T., Vun, C. W., Sánchez-Lavega, A., McGouldrick, K., Horinouchi, T., et al. (2020). A long-lived sharp disruption on the lower clouds of Venus. *Geophysical Research Letters*, *47*(11), e2020GL087221. https://doi.org/10.1029/2020GL087221

Peralta, J., Sánchez-Lavega, A., Horinouchi, T., McGouldrick, K., Garate-Lopez, I., Young, E. F., et al. (2019). New cloud morphologies discovered on the Venus's night during Akatsuki. *Icarus*, *333*, 177–182. https://doi.org/10.1016/j.icarus.2019.05.026

Rayleigh, L. (1880). On the stability, or instability, of certain fluid motions. *Proceedings of the London Mathematical Society*, *9*(1), 57–70. https://doi.org/10.1112/plms/s1-11.1.57

Read, P., Kennedy, D., Lewis, N., Scolan, H., Tabataba-Vakili, F., Wang, Y., et al. (2020). Baroclinic and barotropic instabilities in planetary atmospheres: Energetics, equilibration and adjustment. *Nonlinear Processes in Geophysics*, *27*(2), 147–173. https://doi.org/10.5194/npg-27-147-2020

Ritchie, E. A., & Holland, G. J. (1999). Large-scale patterns associated with tropical cyclogenesis in the Western Pacific. *Monthly Weather Review*, *127*(9), 2027–2043. https://doi.org/10.1175/1520-0493(1999)127<2027:LSPAWT>2.0.CO;2

Sánchez-Lavega, A., Hueso, R., Piccioni, G., Drossart, P., Peralta, J., Pérez-Hoyos, S., et al. (2008). Variable winds on Venus mapped in three dimensions. *Geophysical Research Letters*, *35*(13), L13204. https://doi.org/10.1029/2008GL033817

Satoh, T., Sato, T. M., Nakamura, M., Kasaba, Y., Ueno, M., Suzuki, M., et al. (2017). Performance of Akatsuki/IR2 in Venus orbit: The first year. *Earth Planets and Space*, *69*(1), 154. https://doi.org/10.1186/s40623-017-0736-x

Satoh, T., Vun, C. W., Kimata, M., Horinouchi, T., & Sato, T. M. (2021). Venus night-side photometry with "cleaned" Akatsuki/IR2 data: Aerosol properties and variations of carbon monoxide. *Icarus*, *355*, 114134. https://doi.org/10.1016/j.icarus.2020.114134

Sugimoto, N., Takagi, M., & Matsuda, Y. (2014). Baroclinic instability in the Venus atmosphere simulated by GCM. *Journal of Geophysical Research: Planets*, *119*(8), 1950–1968. https://doi.org/10.1002/2014JE004624

Travis, L. D. (1978). Nature of the atmospheric dynamics on Venus from power spectrum analysis of Mariner 10 images. *Journal of the Atmospheric Sciences*, *35*(9), 1584–1595. https://doi.org/10.1175/1520-0469(1978)035<1584:NOTADO>2.0.CO;2

Vallis, G. K. (2017). *Atmospheric and oceanic fluid dynamics*. Cambridge University Press.